Closed-loop Asymmetric-tip Needle Steering Under Continuous Intraoperative MRI Guidance

Niravkumar A. Patel[1], Tim van Katwijk[2], Gang Li[1], Pedro Moreira[2], Weijian Shang[1], Sarthak Misra[2] and Gregory S. Fischer[1]

***Abstract*— Magnetic resonance imaging (MRI) provides excellent image contrast for various types of tissues, making it a suitable choice over other imaging modalities for various image-guided needle interventions. Furthermore, robot-assistance is maturing for surgical procedures such as percutaneous prostate and brain interventions. Although MRI-guided, robot-assisted needle interventions are approaching clinical usage, they are still typically open-loop in nature due to the lack of continuous intraoperative needle tracking. Closed-loop needle-based procedures can improve the accuracy of needle tip placement by correcting the needle trajectory during insertion. This paper proposes a system for robot-assisted, flexible asymmetric-tipped needle interventions under continuous intraoperative MRI guidance. A flexible needle's insertion depth and rotation angle are manipulated by an MRI-compatible robot in the bore of the MRI scanner during continuous multi-planar image acquisition to reach a desired target location. Experiments are performed on gelatin phantoms to assess the accuracy of needle placement into the target location. The system was able to successfully utilize live MR imaging to guide the path of the needle, and results show an average total targeting error of 2.5±0.47mm, with an average in-plane error of 2.09±0.33mm.**

I. INTRODUCTION

Needle-based percutaneous interventions such as biopsies, brachytherapy, and ablation are some of the most common types of minimally invasive procedures. The success rate of these procedures is closely related to the accuracy of the needle tip placement. Fluoroscopy, computed tomography (CT), ultrasound (US), and magnetic resonance (MR) are the imaging techniques typically used by surgeons to localize the needle tip and the suspected lesion. In the case of prostate biopsy, the gold standard technique is the transrectal ultrasound scan (TRUS) guided biopsy, where continuous US images are used to guide the needle while it is being inserted towards the suspected lesion in the prostate. However, TRUS-guided biopsy has only 32-43% detection rate since lesion visualization in US images is difficult [1]. Whereas, MRI provides more detailed anatomical images than US and an early stage lesion might be visible due to the high soft tissue contrast. But, to perform needle-based procedures using MRI guidance, the surgeon must overcome challenges including a limited workspace, MRI compatibility of instruments, and difficulties of acquiring continuous intraoperative MR images of the region of interest during the intervention.

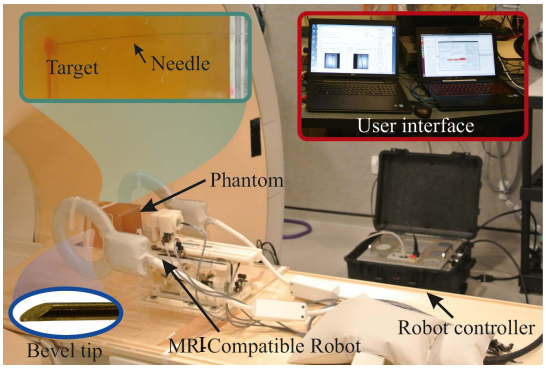

Fig. 1. Overall system setup showing: user interfaces for robot controller application and needle tracking application (inlay, in console room), MRI compatible robot controller (beside scanner), and the MRI compatible robot which resides on the scanner bed beside the phantom and holds the bevel-tipped needle.

The use of robotic systems inside the MRI environment can help the surgeon to perform needle-based procedures with MRI guidance [2]–[6]. Still, most of the procedures proposed so far are still open-loop due to the lack of an effective MRI-based needle tracking method. The development of an autonomous needle tracking system is crucial for the implementation of closed-loop needle insertions. However, MR image acquisition time, difficulties to keep the needle tip in the field of view, and quality of fast and continuous MR images for tracking the needle are issues that make MRI-based needle steering a challenging task. Active needle and catheter tracking techniques were proposed in [7]–[9], but an RF coil has to be placed on the needle tip to be tracked. Just a few works deal with passive tracking. In [10] needle tracking for two-dimensional (2D) MR images is presented while in [11] a system to track the plane of an active loopless-antenna needle is described. Although these systems were used for needle tracking, feasibility of using these methods for closed-loop needle steering has not been evaluated. Using needle tracking for closed-loop flexible needle steering can improve accuracy of needle-based interventions.

The use of flexible bevel-tipped needles instead of conventional rigid needles increases the steerability. The enhanced steerability improves accessibility to a lesion which might be obstructed by structures such as nerves, blood vessels or bones on the insertion path. These needles deflect when

[1]N. A. Patel, G. Li, W. Shang and G. S. Fischer are with the Automation and Interventional Medicine(AIM) Laboratory in the Department of Mechanical Engineering at Worcester Polytechnic Institute, Worcester, MA, USA [napatel, gfischer]@wpi.edu

[2]T. van Katwijk, P. Moreira and S. Misra are with the Surgical Robotics Laboratory(Department of Biomechanical Engineering), University of Twente, Enschede, The Netherlands. S. Misra is also affiliated with the Department of Biomedical Engineering, University of Groningen and University Medical Center Groningen, The Netherlands [s.misra@utwente.nl]

978-1-4244-9270-1/15/$31.00 ©2015 IEEE

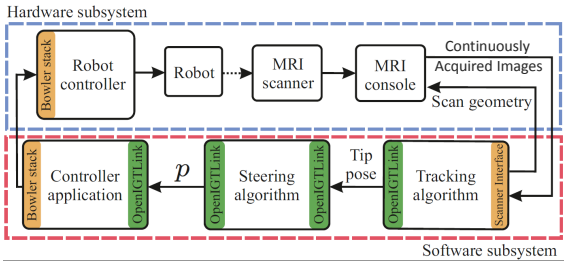

Fig. 2. System architecture showing hardware and software subsystems for control of the robot and the MRI scanner. Communication between the system components uses the OpenIGTLink and Bowler Stack protocols. The steering parameters (p) include the needle rotation angle and insertion depth.

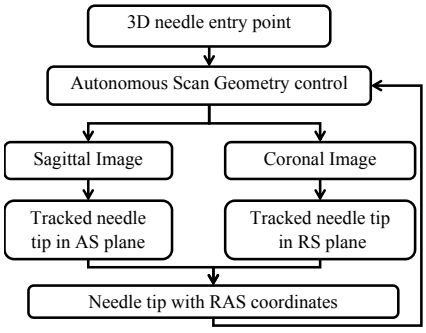

Fig. 3. Flow chart of the needle tracking application workflow. The application tracks the needle tip in alternating sagittal and coronal images and automatically adjusts the scan plane geometry to maintain the needle tip at their cross-section.

they are inserted into soft tissue due to the asymmetric interaction forces between the tissue and the bevel tip. Robotic systems used to insert flexible bevel-tipped needles have been presented using video cameras [12], fluoroscopic images [13], ultrasound images [14] and electromagnetic trackers [15] to provide needle tip position feedback. These systems use needle insertion and rotation around the insertion axis to steer the needle towards a target. In [16] duty-cycled rotations were used to provide different needle curvatures, while in [17] only the natural curvature of the needle was used for steering. A feasibility study of manual steering of a flexible needle in the MR environment was presented in [18], where the manual insertions and rotations induced significant errors. Therefore, using an MRI-compatible robotic system to automate insertion and rotation with MRI-based needle tracking system can result in an accurate MRI-guided bevel-tipped needle steering.

In this paper, a robot-assisted closed-loop flexible needle steering using MR images as feedback is demonstrated. The proposed system consists of an MRI-compatible robot, fast and continuous MR image acquisition, autonomous needle tracking incorporating control of the MRI scan plane geometry, and a needle steering algorithm to insert a flexible bevel-tipped needle towards a pre-defined target as shown in Fig. 1. To the best of our knowledge this is the first time that robot-assisted flexible needle steering is performed using continuous intraoperative MR images for feedback.

II. SYSTEM ARCHITECTURE

The system is composed of: (1) hardware subsystem and (2) software subsystem. Components of the hardware subsystem are: (a) MRI compatible robot, (b) MRI compatible robot controller, and (c) MRI scanner. Components of the software subsystem are: (a) autonomous needle tracking and scan plane control application, (b) robot control application, and (c) needle steering algorithm. Fig. 2 shows the overall system architecture and components of the system.

The hardware subsystem focuses on continuous intraoperative MR image acquisition and needle steering using the robot placed inside the MRI scanner bore. The flexible needle is driven by the MRI-compatible interventional robot designed to place the needle in the tightly-constrained MRI scanner bore. The robot is driven by non-harmonic piezoelectric motors (PiezoMotor PiezoLegs actuators, Uppsala, Sweden). The robot controller located beside the MRI scanner in Fig. 1 is custom developed to be compatible with an MRI environment and provides high-precision closed-loop control of piezoelectric motors, as previously reported in [19].

The software subsystem focuses on autonomously tracking the needle in the most recently acquired MR images, calculating steering parameters, controlling the robot and communication between these components. The connection between the robot controller and the robot control application is established via the fiber optic Ethernet which runs through the patch panel on the wall of the scanner room to eliminate the electrical noise. For the described implementation using a Philips 3T Achieva scanner, the scanner console and the tracking application communicates using the XTC (eXTernal control) [20] Corba Data Dumper to continuously acquire MR images and send the image position and orientation for future scans. Using the most recent images, the needle tracking application calculates the 3D needle position and sends it to the steering algorithm over OpenIGTLink [21] which is an open source protocol for communication among image-guided therapy (IGT) applications. The steering algorithm interpolates all past and current needle positions received from the needle tracking application and calculates insertion and rotation values to steer the needle towards the desired target for each increment. The steering parameters calculated by the steering algorithm are sent to the robot controller application over OpenIGTLink, which are passed to the robot controller over the Bowler communication protocol [22].

III. MR BASED NEEDLE TRACKING

Autonomous needle tracking in MR images is a challenging task as it requires fast and continuous MR image acquisition, visualization, autonomous scan geometry control, and needle tip tracking. Fig. 3 shows the flowchart of the autonomous needle tracking application, where R (right), A (anterior) and S (superior) coordinates are position of the needle tip in scanner coordinates, corresponding with X, Y and Z coordinates, respectively.

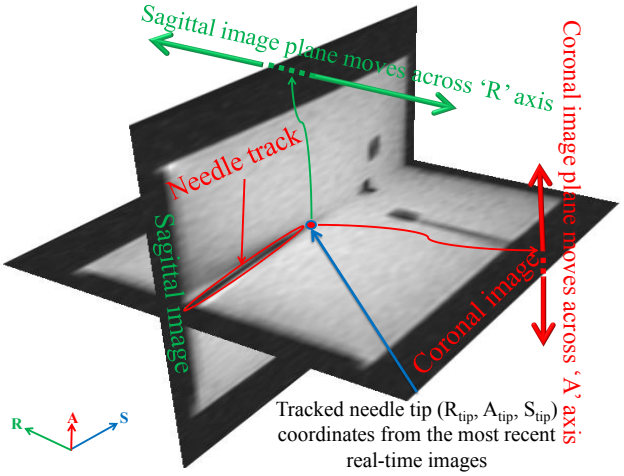

Fig. 4. Scan geometry control showing how the sagittal image is moved Left/Right('R' axis) and coronal image is moved Up/Down ('A' axis) autonomously to ensure that the needle tip is always visible in both images. For sagittal image only the 'R' coordinate of the image position changes, while for the coronal image only the 'A' coordinate of the image position changes.

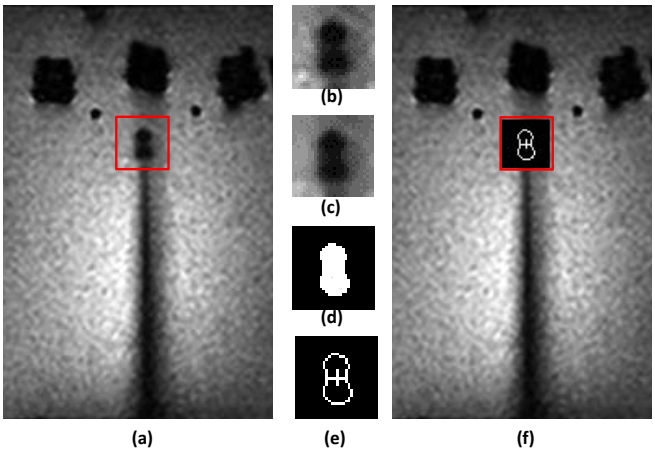

Fig. 5. Autonomous needle tracking: (a) original image, (b) cropped to region of interest, (c) after median blur, (d) after thresholding, (e) after contour detection and center of contour bounding box, and (f) needle tip overlaid on original image.

A. Continuous MR Image Acquisition

The MR images should be of sufficient image quality to detect the needle tip, while being fast enough to provide continuous tracking. To reduce the scanning time, one coronal and one sagittal image is acquired with a slice thickness of 10 mm, resulting in two normal projection images of the needle as shown in Fig. 4. As described in the subsection III-B, the scan geometry is updated continuously to acquire the sagittal and the coronal images one after the other. The thickness of the slice ensures high SNR while ensuring that the needle is maintained in the field of view.

The MRI sequence used for fast image acquisition is Spoiled Gradient Echo sequence T1-FFE (Fast Field Echo). By using T1-FFE, it is possible to obtain an MR image in either sagittal or coronal plane approximately every 750 ms. The T1-FFE sequence parameters used for all the experiments are: TR: 6.9291 ms, TE: 3.37 ms, Flip angle: 5°, FOV (Field of View): 120 X 120 mm, acquisition resolution: 1 X 1 mm and reconstruction resolution: 0.42 X 0.42 mm.

B. Autonomous Scan Geometry Control

Scan geometry for the autonomous tracking application used in this paper is defined as a combination of (1) image orientation (transverse/sagittal/coronal) and (2) image position (R, A, S). The needle tip should be visible in both acquired projection images in order to calculate the 3D position of the tip. Since the slices are 10 mm thick, any deflection beyond that causes the needle tip to go out of the acquired projection images. Therefore, the scan geometry is updated using the located tip position in the most recent projection images in order to keep the needle tip visible all the time. As shown in Fig. 4 the sagittal image is moved along the R-axis based on the needle tip position determined in the most recent coronal image. Likewise, the coronal image is moved along the A-axis based on the needle tip position determined in the most recent sagittal image, maintaining the tip at the cross section.

C. Autonomous needle tracking

Tracking the needle tip is a crucial task for closed-loop needle steering. Using the projection images, the tracking problem is reduced from a 3D volume to two 2D images. As shown in Fig. 5, most recent images are processed to segment the needle tip using image processing operations including median blurring, thresholding and contour detection over the region of interest and tracked needle tip is overlaid on the original images. Overlayed images are displayed to visualize the needle tip position and trajectory using the tracking application presented in Fig. 6. MR images are being acquired all the time and the needle tip is updated every time new set of images are available. The 3D needle tip coordinates are determined by taking 'R' coordinate from the coronal image and 'A' and 'S' coordinates from the sagittal image with an assumption that the 'S' coordinate is same in both images due to the same value for the 'S' coordinate in scan geometries. Combined needle tip (R_{tip}, A_{tip}, S_{tip}) coordinates are sent to the steering algorithm and the scan geometry is updated.

IV. NEEDLE STEERING ALGORITHM

A flexible needle with an asymmetric beveled tip bends as it is inserted into the soft tissue due to the asymmetric interaction forces between the bevel tip and the tissue. The needle is assumed to move along an approximately constant curvature path in the direction corresponding with its bevel tip [23]. Thus the needle can be steered in the 3D space by axially rotating the needle while it is inserted. The steering algorithm defines the axial rotation angle (α) and the insertion step depth needed to steer towards a target based on the needle and target pose.

First, the needle pose (T_{tip}) and target pose (T_{tar}) have to be determined in the global frame. The target pose is

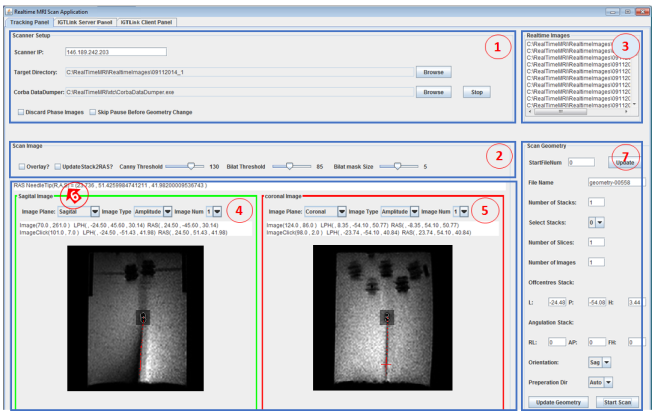

Fig. 6. Autonomous needle tracking application showing: (1) the scanner control interface for configuring the scanner interface, (2) image processing parameters for autonomous tracking, (3) list of all the images received from XTC, (4) the most recent sagittal image, (5) the most recent coronal image, (6) needle tip coordinates from the autonomous tracking algorithm, and (7) scan geometry update interface to autonomously update the scan geometry based on tracked tip location.

considered to be a static location without any rotation and can thus be determined manually by using the MRI user interface. The needle pose is defined by:

$$T_{tip} = \begin{bmatrix} R_{tip} & p_{tip} \\ 0 & 1 \end{bmatrix}$$

where R_{tip} is 3X3 rotation matrix defining the needle tip direction and p_{tip} is 3x1 needle tip position.

The autonomous needle tracking application provides 3D needle tip positions for each insertion step. Consider that the needle trajectory in last N mm of insertion is given as

$$\begin{bmatrix} X \\ Y \\ Z \end{bmatrix} = \begin{bmatrix} x_1 & x_2 & ..... & x_n \\ y_1 & y_2 & ..... & y_n \\ z_1 & z_2 & ..... & z_n \end{bmatrix}$$

Now to estimate the needle pose, line is fit in YZ and XZ planes from the last N mm trajectory using least square and then those lines are used to determine the angle about X and Y axis respectively. Following equations give slope of the lines as 'a' and 'c' in YZ and XZ planes respectively, which are then used to calculate rotation about X and Y axis respectively.

$$Z = a * Y + b \quad \text{and} \quad Z = c * X + d,$$

$$\theta_X = \arctan(a) \quad \text{and} \quad \theta_Y = \arctan(c)$$

To find rotation about Z, current needle rotation is requested from the robot which is defined as θ_Z.
Now needle tip rotation matrix is calculated by combining corresponding rotations about each axis as below,

$$R_{tip} = R_z(\theta_Z) * R_y(\theta_Y) * R_x(\theta_X)$$

The steering algorithm uses the needle and target poses to perform a homogeneous transformation to calculate the axial rotation required to steer the needle towards a predefined target. Fig. 7 shows how the relative rotation angle is

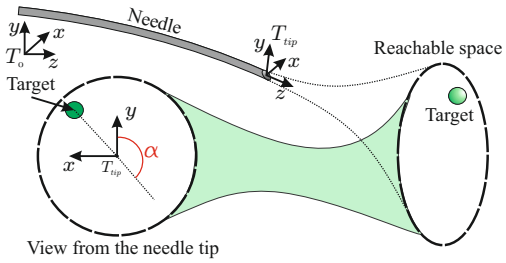

Fig. 7. Needle steering parameter calculations, where α is the rotation angle, T_{tip} is the needle tip frame and T_0 is the global reference frame.

calculated by first defining the target point within the needle coordinate frame, which is given by

$$T_{tip}^{tar} = T_{tip}^{-1} T_{tar},$$

where T_{tip}^{tar} is the target pose in the needle tip coordinate frame.

The angle α provides the relative amount of needle rotation needed to align the needle tip z-axis with the target position, which is determined by:

$$\alpha = \arctan(x, y) + \frac{\pi}{2},$$

where x and y are the coordinates of the target in the needle tip frame (T_{tip}^{tar}). The addition of $\frac{\pi}{2}$ is due to the definition of the used axis system where 0 degrees is aligned with the negative y-axis. The insertion step size for each step can be set beforehand. Ideally the insertion depth for each step should be as small as possible so the rotation angle can be determined continuously. However, smaller steps would increase total insertion time. Also, with the current MR image acquisition frame rate of 1.3 fps, faster insertion would result in less needle position feedback to the steering algorithm and consequently the targeting accuracy would be reduced. Thus a trade-off has to be made between the insertion time and the targeting accuracy.

After each insertion step the updated needle track coordinates from the most recent projection images are requested from the autonomous needle tracking application. The process of determining the rotation angle is repeated until the target is reached.

V. EXPERIMENT AND RESULTS

This section describes the experiments performed to validate the setup and methods used.

A. Experiment Setup

The feasibility of the system workflow and the accuracy of the closed-loop robot-assisted needle steering are assessed with phantom studies, in a Philips 3T MRI scanner, as shown in Fig. 1. A bevel-tipped, solid yet flexible nitinol needle with a diameter of 0.8 mm (21G) and a tip angle of 30° is used in this study. The insertion and rotation of the needle is driven by a 7-DOF MRI-compatible needle placement robot, as described in detail in [3], [24]. The gelatin phantom is made with a mixture of 13% gelatin (Knox, Northfield, USA) and

TABLE I

ACCURACY ASSESSMENT OF STEERING TO 5 TARGETS

No	Target Position[mm]			Final Tip Position[mm]			Error[mm]			Total Error[mm]	In-plane(RA) Error[mm]
	R	A	S	R	A	S	R	A	S		
1	4.162	4.59	81.088	6.402	4.69	82.438	2.24	0.1	1.35	2.62	2.24
2	-0.841	-7.09	81.723	0.919	-6.45	82.653	1.76	0.64	0.93	2.09	1.87
3	-1.248	7.92	77.563	0.802	8.55	78.453	2.05	0.63	0.89	2.32	2.14
4	13.176	0	70.474	14.836	0.14	71.904	1.66	0.14	1.43	2.20	1.67
5	9.171	-5.01	81.727	11.651	-4.55	83.787	2.48	0.46	2.06	3.26	2.52
Mean							2.04	0.39	1.33	2.50	2.09
Standard deviation							0.34	0.26	0.47	0.47	0.33

Note: R, A and S are the coordinates of the needle tip, while RA plane corresponds to axial plane in MRI scanner coordinate system.

87% water. Plastic toothpicks are attached on the container wall to serve as target markers.

The experiments are performed as follows: At the beginning of each insertion the needle is inserted 5 mm into the phantom to determine the initial position of needle tip. Target position on the edge of the markers is selected manually in the MR images. Initial tip and target positions are provided to the steering algorithm. The needle steering is done with constant velocity insertion steps of 3 mm, needle pose is determined using the tracked points within the last 5 mm as described in section IV. Though, needle position is continuously updated by autonomous needle tracking algorithm and sent to the steering algorithm, steering parameters are calculated and sent to the robot controller every 3 mm and insertion is stopped to align the needle to desired steering angle. This process is repeated until the needle tip reaches within 1 mm of the target along the insertion axis. At the end of the insertion, for better accuracy assessment, the final error is manually determined by comparing the actual tip position collected with a standard diagnostic T2-weighted turbo spin echo (T2W-TSE) image (TR= 3030 ms, TE=115 ms, flip angle=90°, slice thickness = 3 mm, FOV: 120 X 120 X 120 mm, acquisition resolution: 0.5 X 0.5 mm and reconstruction resolution: 0.5 X 0.5 mm) with the desired target position. Phantom is shifted to avoid previous needle tracks and a different entry and target point are determined for each insertion.

B. Results

Five needle steering experiments are performed to validate the system. The results of the experiments are summarized in Table I. Based on the selected targets at different locations, the insertion depth varies between 70 mm and 85 mm. The average insertion time is around 12 minutes which includes time for needle alignment and insertion. Fig. 8 shows all the ideal and continuously tracked needle trajectories. The ideal trajectory is computed based on the steering parameters and a deflection model with a curving radius of 300 mm as determined experimentally. The final tip positions of the needle correspond with the desired target points with an average total error of 2.5 mm. In most surgical procedures, error along the insertion axis (S) is not considered as significant compared to the errors in RA plane normal to the needle axis. As shown in Table I, average error in the RA plane is 2.09 mm. A study of manual MRI-guided needle biopsy presented in [25] has shown targeting errors of 5.5 mm to 6.3 mm. Without needle steering, considering curving radius of 300 mm and average insertion depth of 80 mm, maximum error for a straight insertion can be as large as 10.08 mm. Therefore, the average targeting error with closed-loop needle steering presented in this paper can bring benefits to various needle-based interventions.

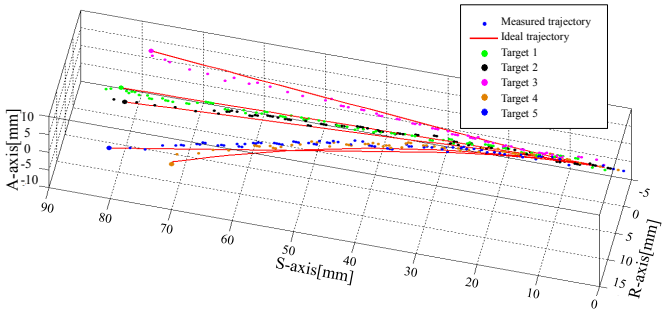

Fig. 8. Ideal and tracked needle trajectories: the ● represents the actual tip positions acquired by the autonomous needle tracking algorithm during the insertion, while ——— represents the ideal needle trajectory generated from the kinematics model

VI. CONCLUSIONS AND FUTURE WORK

This paper presents a closed-loop steering approach for bevel-tipped needles using an MRI-compatible robot and an autonomous needle tracking system. The needle tracking problem is reduced from a 3D volume to a 2D image processing by using the projected images in coronal and sagittal planes. The MRI scan-plane geometry is continuously adjusted to keep the needle tip visible during the insertion, which is essential for tracking the needle tip. This approach provides closed-loop steering of the needle to autonomously reach a target. It is the first time that the closed-loop needle steering using autonomous needle tracking is performed under MRI-guidance. The average targeting errors of 2.5 mm presented in this paper demonstrates feasibility of MRI-guided closed-loop needle-based interventions and shows the potential benefits that a closed-loop flexible needle steering can bring to clinical applications.

Further work will focus on the improvement of the autonomous needle tracking system by implementing an image processing algorithm combined with Kalman filtering to improve the tracking accuracy. With improved tracking algorithm, we will be able to reduce the image slice thickness from 10 mm to 5-7 mm resulting in better visibility of anatomical structures. Also, we plan to improve the control algorithm by implementing on-line needle model estimation. Experiments in biological tissues will be conducted to validate the needle tracking and the steering algorithm in an non-homogeneous environment. Moreover, it is planned to integrate a rapidly exploring random tree (RRT) path planner to calculate the optimal needle path to reach the target while avoiding critical tissue structures. While we will continue to improve our system, the current study demonstrates the feasibility of using MR images to close the steering loop of a flexible bevel-tipped needle and provide autonomous steering towards a target.

ACKNOWLEDGMENT

This work is supported by the National Institutes of Health (NIH) grants R01CA166379 and R01CA111288 through the National Cancer Institute (NCI), and funds from the Dutch Ministry of Economic Affairs and the Province of Overijssel, within the Pieken in de Delta (PIDON) Initiative, Project: MIRIAM (Minimally Invasive Robotics In An MRI environment). We are thankful to Dr. Shaokuan Zheng for his help during all the experiments at the MRI center, University of Massachusetts Medical School.

REFERENCES

[1] J. J. Fütterer, S. Misra, and K. J. Macura, "MRI of the prostate: potential role of robots," *Imaging in Medicine*, vol. 2, no. 5, pp. 583–592, 2010.

[2] R. Seifabadi, I. Iordachita, and G. Fichtinger, "Design of a teleoperated needle steering system for MRI-guided prostate interventions," in *IEEE International Conference on Biomedical Robotics and Biomechatronics (BioRob)*, (Rome, Italy), pp. 793–798, June 2012.

[3] G. Li, H. Su, W. Shang, J. Tokuda, N. Hata, C. M. Tempany, and G. S. Fischer, "A fully actuated robotic assistant for MRI-guided prostate biopsy and brachytherapy," in *SPIE Medical Imaging: Image-Guided Procedures, Robotic Interventions, and Modeling*, p. 8671:867117, 2013.

[4] D. Stoianovici, C. Kim, G. Srimathveeravalli, P. Sebrecht, D. Petrisor, J. Coleman, S. Solomon, and H. Hricak, "MRI-safe robot for endorectal prostate biopsy," *IEEE/ASME Transactions on Mechatronics*, vol. 19, no. 4, pp. 1289–1299, 2014.

[5] M. Schouten, J. Bomers, D. Yakar, H. Huisman, E. Rothgang, D. Bosboom, T. Scheenen, S. Misra, and J. Fütterer, "Evaluation of a robotic technique for transrectal MRI-guided prostate biopsies," *European Radiology*, vol. 22, no. 2, pp. 476–483, 2012.

[6] S. Abdelaziz, L. Esteveny, L. Barbé, P. Renaud, B. Bayle, and M. de Mathelin, "Development of a MR-compatible cable-driven manipulator: Design and technological issues," in *IEEE International Conference on Robotics and Automation (ICRA)*, (St. Paul, USA), pp. 1488–1494, 2012.

[7] J. Krücker, S. Xu, N. Glossop, A. Viswanathan, J. Borgert, H. Schulz, and B. J. Wood, "Electromagnetic tracking for thermal ablation and biopsy guidance: clinical evaluation of spatial accuracy," *Journal of Vascular and Interventional Radiology*, vol. 18, no. 9, pp. 1141–1150, 2007.

[8] D. A. Leung, J. F. Debatin, S. Wildermuth, N. Heske, C. L. Dumoulin, R. D. Darrow, M. Hauser, C. P. Davis, and G. K. von Schulthess, "Real-time biplanar needle tracking for interventional MR imaging procedures.," *Radiology*, vol. 197, no. 2, pp. 485–488, 1995.

[9] S. Xu, J. Kruecker, B. Turkbey, N. Glossop, A. K. Singh, P. Choyke, P. Pinto, and B. J. Wood, "Real-time MRI-TRUS fusion for guidance of targeted prostate biopsies," *Computer Aided Surgery*, vol. 13, no. 5, pp. 255–264, 2008.

[10] E. Kochavi, D. Goldsher, and H. Azhari, "Method for rapid MRI needle tracking," *Magnetic Resonance in Medicine*, vol. 51, no. 5, pp. 1083–1087, 2004.

[11] S. Sathyanarayana, P. Aksit, A. Arepally, P. V. Karmarkar, M. Solaiyappan, and E. Atalar, "Tracking planar orientations of active MRI needles," *Journal of Magnetic Resonance Imaging*, vol. 26, no. 2, pp. 386–391, 2007.

[12] M. Bernardes, B. Adorno, P. Poignet, and G. Borges, "Robot-assisted automatic insertion of steerable needles with closed-loop imaging feedback and intraoperative trajectory replanning," *Mechatronics*, vol. 23, no. 6, pp. 630 – 645, 2013.

[13] A. Majewicz, T. Wedlick, K. Reed, and A. Okamura, "Evaluation of robotic needle steering in ex vivo tissue," in *IEEE International Conference on Robotics and Automation (ICRA)*, (Anchorage, USA), pp. 2068–2073, 2010.

[14] G. J. Vrooijink, M. Abayazid, S. Patil, R. Alterovitz, and S. Misra, "Needle path planning and steering in a three-dimensional non-static environment using two-dimensional ultrasound images," *International Journal of Robotics Research (In Proof)*, vol. 33, no. 10, pp. 1361–1374, 2014.

[15] S. Patil, J. Burgner, R. Webster, and R. Alterovitz, "Needle steering in 3-d via rapid replanning," *IEEE Transactions on Robotics*, vol. 30, pp. 853–864, Aug 2014.

[16] D. S. Minhas, J. A. Engh, M. M. Fenske, and C. N. Riviere, "Modeling of needle steering via duty-cycled spinning," in *Annual International Conference of the IEEE Engineering in Medicine and Biology Society (EMBC)*, (Lyon, France), pp. 5432 – 5435, August 2007.

[17] M. Abayazid, R. J. Roesthuis, R. Reilink, and S. Misra, "Integrating deflection models and image feedback for real-time flexible needle steering," *IEEE Transactions on Robotics*, vol. 29, no. 2, pp. 542 – 553, 2013.

[18] P. Moreira, G. van de Steeg, F. van der Heijden, J. J. Fütterer, and S. Misra, "A preliminary evaluation of a flexible needle steering algorithm using magnetic resonance images as feedback," in *IEEE International Conference on Biomedical Robotics and Biomechatronics (BioRob)*, (São Paulo, Brazil), pp. 314–319, 2014.

[19] H. Su, D. C. Cardona, W. Shang, A. Camilo, G. A. Cole, D. C. Rucker, R. J. Webster, and G. S. Fischer, "A MRI-guided concentric tube continuum robot with piezoelectric actuation: a feasibility study," in *IEEE International Conference on Robotics and Automation (ICRA)*, (St. Paul, USA), pp. 1939–1945, 2012.

[20] J. Smink, M. Häkkinen, R. Holthuizen, S. Krueger, M. Ries, Y. Berber, C. Moonen, M. Köhler, and E. Vahala, "external control (xtc): a flexible, real-time, low-latency, bi-directional scanner interface," in *Proceedings of the International Society of Magnetic Resonance Medicine*, p. 1755, 2011.

[21] J. Tokuda, G. S. Fischer, X. Papademetris, Z. Yaniv, L. Ibanez, P. Cheng, H. Liu, J. Blevins, J. Arata, A. J. Golby, *et al.*, "Openigtlink: an open network protocol for image-guided therapy environment," *The International Journal of Medical Robotics and Computer Assisted Surgery*, vol. 5, no. 4, pp. 423–434, 2009.

[22] Neuronrobotics, "Bowler communications system," 2010.

[23] R. J. W. III, J. S. Kim, N. J. Cowan, G. S. Chirikjian, and A. M. Okamura, "Nonholonomic modeling of needle steering," *The International Journal of Robotics Research*, vol. 25, no. 5-6, pp. 509–525, 2006.

[24] H. Su, W. Shang, G. Cole, G. Li, K. Harrington, A. Camilo, J. Tokuda, C. M. Tempany, N. Hata, and G. S. Fischer, "Piezoelectrically actuated robotic system for MRI-guided prostate percutaneous therapy," *IEEE/ASME Transactions Mechatronics(in press)*, 2014.

[25] P. Blumenfeld, N. Hata, S. DiMaio, K. Zou, S. Haker, G. Fichtinger, and C. Tempany, "Transperineal prostate biopsy under magnetic resonance image guidance: a needle placement accuracy study," *Journal of Magnetic Resonance Imaging*, vol. 26, no. 3, pp. 688–694, 2007.